Direct observation of transitions between surface-dominated and bulk diffusion regimes in nanochannels

Nicolas F.Y. Durand,[*†‡] Claudio Dellagiacoma,[§‡] Raphaël Goetschmann,[†] Arnaud Bertsch,[†]

Iwan Märki,[§] Theo Lasser,[§] and Philippe Renaud[†]

Microsystems Laboratory and Biomedical Optics Laboratory, Swiss Federal Institute of Technology (EPFL), Lausanne, Switzerland

* To whom correspondence should be addressed. E-mail: nicolas.durand@epfl.ch

[†] Microsystems Laboratory

[§] Biomedical Optics Laboratory

[‡] These authors contributed equally to this work.

Diffusion of charged proteins in liquid-filled nanometer-sized apertures with charged surfaces has been investigated with fluorescence correlation spectroscopy (FCS). Based on a 2D multi-component diffusion model, key parameters like the number of molecules diffusing freely inside the nanochannel or interacting with the surfaces together with the specific diffusion parameters could be extracted. Different regimes of diffusion have been observed and described by a model which takes into account the steric exclusion, the reversible surface adsorption of the biomolecules and the exclusion-enrichment effect due to the charge of the proteins and to the ionic strength of the solution. Conditions where the diffusion of proteins through nano confined spaces can be of the same magnitude as in the bulk were both predicted and experimentally verified.

Recent technological advances in nanofluidics have contributed to new insights in the understanding of fluid transport in and close to nanometer-sized objects with at least one characteristic dimension below 100nm[1]. This research in nanofluidics is particularly well suited for the detection, identification, and dynamic study of single molecules in various conditions. Nanofluidics phenomena[2] such as electrokinetic effects due to the electrical double layer (EDL), the induced redistribution of the electrical potential including the associated surface charge density[3] and surface conductance[4] and the exclusion-enrichement effect[5] are some of the well-known properties, which affect the particular diffusion of biomolecules in highly confined spaces. During the 1980s, the steric exclusion was observed by measuring hindered transport of neutral spheres through pores, giving a deeper understanding of the effects of solute concentration on partitioning and transport coefficients[6-8]. An even stronger decrease of the effective diffusion coefficient of proteins diffusing through nanochannels, due to interactions with surfaces has been recently reported[9-12]. However accurate models of the concentration partitioning and of the diffusion reduction in such conditions are still missing.

In this study, we supply a theoretical model describing the concentration of proteins inside nano-confinements, taking into account the steric exclusion, the presence of reversibly adsorbed molecules on surfaces and the exclusion-enrichment effect. Based on single molecule detection experiments by

fluorescence correlation spectroscopy (FCS), we demonstrate the different diffusion regimes governed by the solution characteristics (ionic strength, pH, charge and concentration of proteins, etc.) and provide evidence for our proposed diffusion model. Therefore, this study presents a new step for a deeper understanding of the transport of charged molecules in nanofluidics.

The experimental set-up is depicted in figure 1a, the nanochannel-device used in the experiment consists of 2 microchannels crosslinked by a thin nanochannel (height h = 50nm, width w = 10μm, length l = 30μm). Solutions containing fluorescently labeled proteins are injected in both microchannels and measurements are performed as soon as the system is at equilibrium, meaning that all channels are completely filled. External negative pressure applied to the outlet ports allow a precise fine tuning of the flows in each microchannel as well as in the nanochannel.

THEORY

Effective concentration in a nanochannel. For solutes that are large enough to behave as hydrodynamic particles, the constrained space of a nanochannel causes the molecular friction coefficient to exceed its maximum value and leads to steric exclusion. This kind of hindered diffusion has been extensively studied with neutral spheres in cylindrical nanopores[8, 13-16]. The equilibrium partitioning of solute concentration between inside and outside a nanoslit, assuming there is no surface close to the measurement volume outside the nanochannel, is given by[8, 17]:

$$\Phi = \frac{\langle c_{nS} \rangle}{c_0} = \int_0^{(1-\lambda)} e^{-\frac{E(\beta)}{k_B T}} d\beta \qquad (1)$$

where $<c_{nS}>$ is the mean concentration of solute in the nanochannel and c_0 the concentration of solute in the bulk. λ is defined as the ratio of the solute diameter d_s to nanochannel height h ($\lambda = d_s/h$) and $\beta = 2z/h\text{-}1$ is the dimensionless z position (z is the projection axis parallel to the height). E is a potential describing long range interactions between the solute and the nanochannel walls which are here assumed to depend only on the z position, k_B is the Bolzmann constant and T the temperature in Kelvin. Equation 1 indicates that when the size of the particles is close to the height of the channel, a decrease of the solute concentration is expected within the nanochannel.

In micro and nanofluidics, the surface to volume ratio is high and the total concentration inside the confined space is a function of the number of molecules in the bulk and of the molecules adsorbed on the nanochannel surfaces. The Langmuir isotherm model[18], which describes reversible adsorption, can be used to define the concentration in the nanochannel taking into account both the molecules in the free-diffusion space (bulk) of the nanochannel and those adsorbed on the walls:

$$\langle c_{nS} \rangle = \left(1 + 2\frac{\Gamma_0}{N_A \cdot h} \right) \cdot c_0 \cdot \Phi \qquad (2)$$

where N_A is the Avogadro constant, the effective steady-state surface concentration Γ_0 is a function of the full coverage surface concentration Γ_{max}, and is also governed by the binding and dissociation constants k_{on} and k_{off}:

$$\Gamma_0 = \frac{k_{on} c_0}{k_{on} c_0 + k_{off}} \cdot \Gamma_{max} \qquad (3)$$

The bulk-surface partitioning cofactor χ is defined as:

$$\chi = 1 + 2\frac{\Gamma_0}{N_A \cdot h} = 1 + \frac{2\Gamma_{max}}{N_A \cdot h} \cdot \frac{k_{on}}{k_{on} \cdot c_0 + k_{off}} \qquad (4)$$

To take into account the electrostatic interactions between charged molecules and charged surfaces as well as the interactions of the solute with the electrical double layer (EDL), depending on the ionic strength of the solution c_i, a model given by Plecis *et al*[5] describing the exclusion-enrichment effect was used. This model introduces a partitioning coefficient Φ_β, which takes into account the electrostatic effects and the interactions with the EDL, but ignores the steric exclusion due to the solute size, as well as the adsorption effect:

$$\Phi_\beta = \frac{1}{h} \int_0^h e^{-\frac{q\Psi(z)}{k_B T}} dz \qquad (5)$$

where q is the net charge of the solute and $\Psi(z)$ is the Debye-Hückel approximation for the electrical potential between two infinite planar surfaces[19]:

$$\psi(z) = \zeta \frac{\cosh((h/2 - z)/\lambda_D)}{\cosh(h/2\lambda_D)} \qquad (6)$$

where ζ is the zeta potential and λ_D the EDL thickness corresponding to the Debye screening length, in a 1:1 electrolyte solution[5]:

$$\lambda_D = \sqrt{\frac{\varepsilon_0 \varepsilon_r RT}{2F^2 c_i}} \qquad (7)$$

where ε_0 is permittivity of vacuum, ε_r the dielectric constant of the medium, R the molar gas constant and F the Faraday constant.

Combining these contributions (adsorption, steric exclusion and electrostatic interactions) by combining equations 1, 4 and 5, the equilibrium partitioning coefficient for solute concentration between inside and outside a nanochannel Φ_{nS} can be defined as

$$\Phi_{nS} = \frac{\langle c_{nS} \rangle}{c_0} = \frac{\chi}{h} \int_0^{h(1-\lambda)} e^{-\frac{q\Psi(z)}{k_B T}} dz \qquad (8)$$

When the solute is not charged, as is the case at the isoelectrical point (pI) for proteins, the charge q is zero and equation 8 is reduced to

$$\Phi_{nS} = (1-\lambda)\left(1 + \frac{2\Gamma_{max}}{N_A \cdot h} \cdot \frac{k_{on}}{k_{on} \cdot c_0 + k_{off}}\right) \qquad (9)$$

Effective diffusion in a nanoconfinement. In nano-confined spaces, solute molecules undergo diffusion due to Brownian motion but can also adsorb at the channel walls due to the high surface to volume ratio of the nano-confinement. The Stokes-Einstein equation[20] can be used to estimate the bulk diffusion coefficient D_{bulk} of spherical particles of radius r_s (and by extension of globular proteins) in aqueous solutions:

$$D_{bulk} = \frac{k_B T}{6\pi\eta r_s} \qquad (10)$$

where η is the solvent viscosity. The diffusion time τ_{bulk} is related to the diffusion coefficient D_{bulk} by[21]:

$$\tau_{bulk} = \frac{r_{xy}^2}{4D_{bulk}} \qquad (11)$$

where r_{xy} is the radius of the observed cylindrical volume. Proteins may also adsorb on surfaces which can result in an increased diffusion time through a given volume. The Langmuir isotherm model gives an expression of the time of interaction τ_{surf}[22, 23]:

$$\tau_{surf} = \frac{1}{k_{off}} \tag{12}$$

This effective diffusion time can be expressed as a weighted arithmetic mean of the diffusion times of freely diffusing molecules in the bulk and at reversibly adsorbed molecules on the surfaces:

$$\tau_{eff} = \frac{N_{bulk} \cdot \tau_{bulk} + N_{surf} \cdot \tau_{surf}}{N_{bulk} + N_{surf}} \tag{13}$$

The effective diffusion time τ_{eff} can be determined with our FCS measurements. The effective diffusion coefficient D_{eff} is related to τ_{eff} by:

$$D_{eff} = \frac{r_{xy}^2}{4\tau_{eff}} \tag{14}$$

Overall, these are the dominant contributions to an effective diffusion coefficient which is strongly decreased when measuring the diffusion of proteins in nano-confinements[9, 12, 24].

Fluorescence Correlation Spectroscopy. Fluorescence Correlation Spectroscopy (FCS) allows to access across the fluctuation analysis of fluorescently-labeled single biomolecules static and dynamic molecular parameters such as the mean number of molecules and their diffusion behaviour[21, 25-27]. The classical FCS model for a free 3D diffusion of a single molecular component (ignoring the triplet population) is given by[28]:

$$G(\tau) = \frac{1}{N}\left(1 - \frac{I_B}{I_{tot}}\right)^2 \frac{1}{1+\frac{\tau}{\tau_D}} \sqrt{\frac{1}{1+\omega^2 \frac{\tau}{\tau_D}}} + 1 \tag{15}$$

Where $G(\tau)$ is the autocorrelation function (ACF), N is the number of molecules in the sampling volume and τ_D the characteristic time of diffusion across the illuminated sampling volume. The factor $(1\text{-}I_B/I_{tot})^2$ corrects for a uncorrelated background intensity I_B, with I_{tot} being the total intensity including I_B [29]. The aspect ratio ω of the sampling volume is defined as the ratio between the height $2r_z$ and the

width $2r_{xy}$ of the detection volume $\omega = r_z/r_{xy}$. In a nanochannel, the detection volume is approximated by a cylinder of small height compared to its diameter. Consequently $r_z << r_{xy}$ and ω tends to zero: the square-root term can then be neglected leading to a 2D FCS model[25]. Figure 1b and c shows the difference between the FCS detection volumes of freely 3D diffusing particles (fig 1b) and of confined 2D diffusing particles inside a nanochannel (fig 1c).

Our proposed FCS model for the measurements inside the nanochannel integrates a 2D multi-component diffusion model with two different populations of particles: biomolecules diffusing freely through the nanochannel (N_{bulk}, τ_{bulk}) and biomolecules interacting with the channel surfaces (N_{surf}, τ_{surf}):

$$G(\tau) = \left(1 - \frac{I_B}{I_{tot}}\right)^2 \left[\frac{N_{bulk}}{\left(N_{bulk} + N_{surf}\right)^2} \frac{1}{1 + \frac{\tau}{\tau_{bulk}}} + \right.$$

$$\left. + \frac{N_{surf}}{\left(N_{bulk} + N_{surf}\right)^2} \frac{1}{1 + \left(\frac{\tau}{\tau_{surf}}\right)^{\alpha}} \right] + 1 \qquad (16)$$

where the coefficient α is a constant retention parameter, depending mainly on the geometry of the nanochannel. This phenomenological retention parameter takes into account the modified diffusion behavior of reversibly adsorbed particles. Best fittings of autocorrelation curves have allowed determining that α is an exponential term, in a similar way to the obstruction diffusion parameter which is widely used in anomalous diffusion in biology[30, 31]. In this first model, the triplet state population has been ignored, but it will be considered in detail in a forthcoming publication. Due to the low concentration of charged biomolecules, interactions between particles have been neglected.

EXPERIMENTAL SECTION

Device microfabrication. Cleanroom microfabrication processes have been used to produce the fluidic chips on which the experiments have been carried out. Microchannels have been wet-etched on a 200µm thick Pyrex wafer using standard lift-off techniques, and a 50nm layer of amorphous silicon, used to define the height of the nanochannel was sputtered and structured by plasma etching. A second

Pyrex wafer containing access holes (drilled by sandblasting), was anodically bonded onto the first wafer. Finally the wafers have been diced into individual chips. The nanochannel has the following dimensions: height h = 50nm, width w = 10μm, and length l = 30μm.

The solutions containing proteins are injected in the microchannels through the inlets. The liquids are driven by air aspiration controlled using air-pressure regulators (Bellofram Corp., Newell, WV) from 0 to -800mbars. For all measurements, flow conditions have been chosen where there is no flow across the nanochannel.

Measurement instrument. The FCS experiments have been performed with a ConfoCor microscope (Carl Zeiss, Jena). The laser beam size in the sample has been adjusted by varying the laser beam size in front of the microscope (Objective Olympus UApo 340; NA 1.15; 40x water immersion).The measured spot size was r_{xy} = 420nm at a wavelength of 632.8 nm (HeNe). The nanofluidic setup was placed on a xyz table with a resolution of 1μm. The autocorrelation (ALV correlator) have been transferred to a computer and have been analyzed with FCS Access ConfoCor Control Program 1.2.1.1 (Zeiss) and custom made Matlab code R2006a (MathWorks, Inc).

Materials. To investigate and characterize the hindered diffusion of proteins we used wheat germ agglutinin labeled with Alexa Fluor® 633 (WGA, from Molecular Probes). WGA has a molecular mass of 38kDa, an isoelectric point (pI) around 4, and a free diffusion coefficient in water[32] D_{bulk} = $7.6(\pm 0.3)\cdot 10^{-11} m^2/s$.

These WGA proteins have been added to potassium chloride (KCl) solutions, which have been prepared with different dilutions (10^{-5}M to 10^{-1}M) by addition of deionized water (18MΩ·cm). The concentration of the WGA proteins is 50nM in all prepared solutions, which were adjusted to pH = 7 by addition of small amount of HCl. For all experiments, no pre-treatment was performed on the chip in which the solutions have been directly injected. All solutions were prepared and degassed before use at a room temperature T = 25°C.

RESULTS AND DISCUSSION

A series of experiments have been carried out to evaluate the number of molecules and the diffusion time of the WGA proteins at two different locations: i) inside the reservoirs for measuring the bulk values (away from chip surfaces) and ii) inside the nanochannel for measuring the diffusion parameters inside the channel.

After filling the microchannels, the solution entered the nanochannel by capillarity, resulting in a slow change of fluorescence intensity inside the nanochannel. All measurements have been started once the fluorescence intensity reached a steady-state.

3D diffusion of WGA. The fluorescence fluctuations of a 50nM solution of WGA proteins placed on-chip, in one of the reservoirs were measured with the FCS setup and a diffusion time of τ_{bulk} = 0.6(±0.02)ms was obtained by fitting the experimental data to equation 15, as this bulk experiment corresponds to standard 3D free diffusion of a single component. From this value of τ_{bulk}, the diffusion coefficient D_{bulk} = 7.35(±0.3)·10^{-11}m^2/s was obtained from eq 14 with r_{xy} = 420nm, which corresponds to the radius of the detection area. This value is very close to the diffusion coefficient of WGA in water reported by Munson *et al.*[32] of D_{bulk} = 7.6(±0.3)·10^{-11}m^2/s.

Exclusion of proteins at low ionic strength. The curve in figure 2a shows the mean fluorescent intensity I_{tot} measured in different ionic conditions in the 50nm high nanochannel. Pyrex surfaces in contact with aqueous solutions are negatively charged, which electrostatically repulses negatively charged WGA proteins. A strong decrease of I_{tot} is observed when increasing the EDL by reducing the ionic concentration in the nanochannel, which is coherent with eq 8. In figure 2a, eq 8 is fitted on the experimental data points with d_s = 4nm, q = -e and $\zeta = 30 \cdot 10^{-3} \cdot \log(c_i)$ as measured by Kosmulski *et al.*[33]. For values of the ionic concentration lower than 10^{-4}M, the EDL overlap (EDLO) is observed; only the uncorrelated background intensity was measured, which corresponds to the exclusion of the proteins from the nanochannel.

2D diffusion of WGA in the 50nm nanochannel. The autocorrelation curves obtained when WGA proteins are diffusing inside the nanochannel for different values of the ionic strength of the solution are presented in figure 2b. As all experiments are performed with identical nanochannels, at a constant

value of pH and using solutions of 50nM WGA proteins, while ionic concentration is changed, eq 16 can be used to fit each set of experimental data points with τ_{bulk}, τ_{surf} and α being constant parameters. The values of τ_{bulk} = 0.6(±0.02)ms was measured independently as presented in a previous paragraph and τ_{surf} = 10(±2)ms and α = 0.45±0.1 were obtained from fitting of all FCS measurements inside the nanochannel.

All other parameters being kept constant in eq 16, the fit of the data to the autocorrelation function allows to estimate the values of N_{bulk} and N_{surf}, which correspond to the average number of WGA proteins diffusing freely or interacting with the nanochannel walls respectively. A good agreement between the measurements and eq 16 has been obtained in all cases, as shown in figure 2b for three values of the ionic concentration.

Figure 3 shows the evolution of the estimated values of N_{bulk} and N_{surf}, as a function of the ionic strength of the solution.

At high ionic strength (for $c_i > 10^{-1}$M) a large number of proteins are present in the nanochannel and most of them interact with the walls (N_{bulk} is close to zero). This situation is schematically described in fig 4a: As the ionic concentration is high, the EDL is small and does not prevent the interaction between the proteins and the walls.

When the ionic strength of the solution decreases from 10^{-1}M to $4 \cdot 10^{-4}$M, the number of proteins present in the nanochannel decreases strongly. The EDL induces an electrostatic repulsion of the negatively charged WGA proteins, and this effect is amplified as the EDL becomes larger. As depicted in Fig 4b, the number of proteins reaching the walls decreases while the number of molecules diffusing freely in the bulk of the nanochannel increases.

For values of the ionic strength close to $4 \cdot 10^{-4}$M, the number of molecules interacting with the walls is close to zero. As presented in Fig 4c, the proteins are maintained away from the channel walls by the large dimension of the EDL. However, as there is no EDL overlap, a small, but significant amount of proteins enters the nanochannel.

When decreasing further the ionic strength, the number of molecules interacting with the surfaces increases again, while the molecules diffusing in the bulk of the nanochannel decreases to zero. As presented in Fig 4d, this corresponds to a case where there is not yet an overlap of the EDL. Only a small number of proteins can enter the nanochannel, but they are no longer confined to the center by electrostatic forces and consequently interact with the surfaces. In that case, the autocorrelation functions measured were similar to the ones measured for high ionic strength.

Finally, for ionic strength lower than 10^{-4}M, there is an exclusion of the proteins from the nanochannel, as there is an overlap of the EDL.

Figure 5 shows the effective times of diffusion τ_{eff} which have been calculated with eq 13 using N_{bulk} and N_{surf} values reported in figure 3. As expected, at high ionic strength τ_{eff} is close to τ_{surf} as all proteins interact with the walls of the nanochannel because of the limited extension of the EDL and the large surface to volume ratio of the channel. When increasing the EDL, the effective time of diffusion decreases until reaching a minimal value close to τ_{bulk}. This corresponds to the case depicted in Fig 4c where the proteins do no longer reach the walls of the nanochannel due to size of the EDL, and resulting in a diffusion of proteins almost as fast as in the bulk in such specific ionic conditions. Finally, at very low ionic concentration close to the EDLO, the rare proteins which may enter the nanochannel have a diffusion time close to τ_{surf}.

CONCLUSION

Many technologies have recently been developed to exploit the exclusion or the enrichment of particles in confined area, particularly for biotechnology applications[34], however, the diffusion through such artificial structures is still largely misunderstood.

In this work, we have demonstrated that hindered proteins concentration and diffusion can be measured directly inside a nanochannel with a FCS measurement unit. Our model for the prediction of the concentration in a nanochannel takes into account the steric exclusion as well as interactions of biomolecules with the surfaces and the exclusion-enrichment effect due to the electrical double layer and to the charge of the proteins. We propose a model for the FCS autocorrelation functions, which has

been used to estimate the number of molecules diffusing freely inside the nanochannel and the number of molecules interacting with the surfaces. The measurements performed at different ionic strengths showed different regimes of diffusion and highlighted that for a specific EDL thickness, the diffusion of proteins through a nanochannel can be almost as high as in the bulk.

The models to predict proteins concentration and diffusion in nano confined spaces presented in this paper can be easily used to get a better understanding of on-chip, membranes separation or proteomic processes. We believe that they will help to get a better understanding of fundamental nanofluidic physics in order to develop further biological and biomedical applications.

ACKNOWLEDGMENTS

This work was partially supported by Swiss National Foundation (FNS) grant n°200021-111790. Cleanroom processing was performed at the EPFL Center of MicroNanoTechnology (CMI). Authors wish to thank Erica Martin-Williams for reviewing the manuscript.

REFERENCES

(1) Eijkel, J. C. T.; Van den Berg, A. *Microfluid. Nanofluid.* **2005**, *1*, 249-267.

(2) Schoch, R. B. *Rev. Mod. Phys.* **2008**, *80*, 839-883.

(3) Schoch, R. B.; Philippe, R. *Appl. Phys. Lett.* **2005**, *86*, 253111-253113.

(4) Durand, N. F. Y.; Renaud, P. *Lab Chip* **2009**, *9*, 319-324.

(5) Plecis, A.; Schoch, R. B.; Renaud, P. *Nano lett.* **2005**, *5*, 1147-1155.

(6) Smith Iii, F. G.; Deen, W. M. *J. Colloid. Interf. Sci.* **1980**, *78*, 444-465.

(7) Smith Iii, F. G.; Deen, W. M. *J. Colloid. Interf. Sci.* **1983**, *91*, 571-590.

(8) Deen, W. M. *AIChe J.* **1987**, *33*, 1409-1425.

(9) Durand, N. F. Y.; Bertsch, A.; Todorova, M.; Renaud, P. *Appl. Phys. Lett.* **2007**, *91*, 203106-203103.

(10) Lyon, W. A.; Nie, S. *Anal. Chem.* **1997**, *69*, 3400-3405.

(11) Schlessinger, J.; Koppel, D. E.; Axelrod, D. *P. Natl. Acad. Sci. USA* **1976**, *73*, 2409-2413.

(12) Pappaert, K.; Biesemans, J.; Clicq, D.; Vankrunkelsven, S.; Desmet, G. *Lab Chip* **2005**, *5*, 1104-1110.

(13) Dechadilok, P.; Deen, W. M. *Ind. Eng. Chem. Res.* **2006**, *45*, 6953-6959.

(14) Shao, J.; Baltus, R. E. *AIChE J.* **2000**, *46*, 1149-1156.

(15) Ladero, M.; Santos, A.; Garcia-Ochoa, F. *Chem. Eng. Sci.* **2007**, *62*, 666-678.

(16) Anderson, J. L.; Quinn, J. A. *Biophys. J.* **1974**, *14*, 130-150.

(17) Pawar, Y.; Anderson, J. L. *Ind. Eng. Chem. Res.* **1993**, *32*, 743-746.

(18) Reinmuth, W. H. *J. Phys. Chem.* **1961**, *65*, 473-476.

(19) Hunter, R. J. *Zeta Potential in Colloid Science, Principles and Applications*; Academic Press: London, 1981.

(20) Einstein, A.; Furth, R.; Cowper, A. D. *Investigations on the Theory of the Brownian Movement*; Courier Dover Publications: New York, 1956.

(21) Schwille, P.; Haustein, E. *Fluorescence Correlation Spectroscopy, An Introduction to its Concepts and Applications*; Experimental Biophysics Group, Max-Planck-Institute for Biophysical Chemistry: Göttingen, Germany, 2004.

(22) Wirth, M. J.; Legg, M. A. *Annu. Rev. Phys. Chem.* **2007**, *58*, 489-510.

(23) Hanasaki, I.; Takahashi, H.; Sazaki, G.; Nakajima, K.; Kawano, S. *J. Phys. D: Appl. Phys.* **2008**, *41*.

(24) Takmakov, P.; vlassiouk, I.; Smirnov, S. *Analyst* **2006**, *131*, 1248-1253.

(25) Krichevsky, O.; Bonnet, G. *Rep. Prog. Phys.* **2002**, *65*, 251-297.

(26) Craighead, H. G.; Stavis, S. M.; Samiee, K. T. *Lect. Notes Phys.* **2007**, *711*, 271-301.

(27) Leutenegger, M.; Gösch, M.; Perentes, A.; Hoffmann, P.; Martin, O. J. F.; Lasser, T. *Opt. Express* **2006**, *14*, 956-969.

(28) Aragón, S. R.; Pecora, R. *J. Chem. Phys.* **1976**, *64*, 1791-1803.

(29) Koppel, D. E. *Phys. Rev. A* **1974**, *10*, 1938-1945.

(30) Wachsmuth, M.; Waldeck, W.; Langowski, J. *J. Mol. Biol.* **2000**, *298*, 677-689.

(31) Saxton, M. J.; Jacobson, K. *Annu. Rev. Bioph. Biom.* **1997**, *26*, 373-399.

(32) Munson, M. S.; Hawkins, K. R.; Hasenbank, M. S.; Yager, P. *Lab Chip* **2005**, *5*, 856-862.

(33) Kosmulski, M.; Matijevic, E. *Langmuir* **1992**, *8*, 1060-1064.

(34) Schmuhl, R.; Nijdam, W.; Sekulic, J.; Chowdhury, S. R.; van Rijn, C. J. M.; van den Berg, A.; ten Elshof, J. E.; Blank, D. H. A. *Anal. Chem.* **2005**, *77*, 178-184.

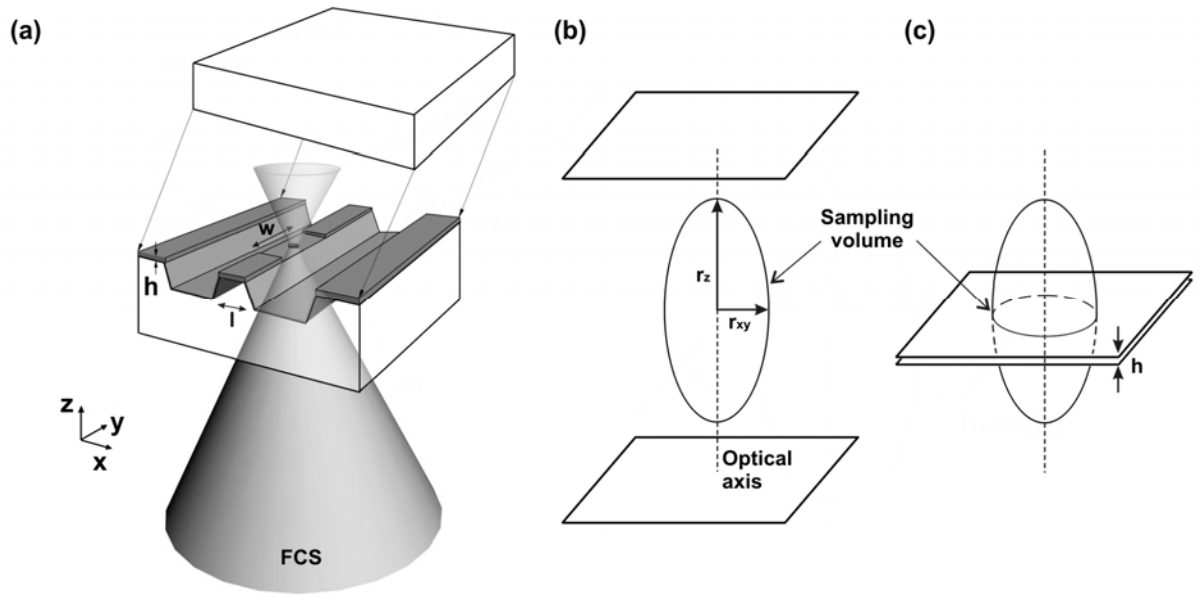

Figure 1. Nanofluidic device using fluorescence correlation spectroscopy for the detection of proteins. (a) 3D schematic of the nanofluidic system (not to scale) made of 2 microchannels linked by a nanochannel. A 50nm amorphous silicon layer, sandwiched between 2 Pyrex wafers, defines the height of the nanochannel. (b) FCS detection volume in the case of 3D freely diffusing biomolecules. (c) FCS detection volume of 2D confined diffusing molecules between two walls (when $h_{nS} << 2r_z$), such as in the case of the nanochannel. The ellipsoidal detection volume, of height $2r_z$ and width $2r_{xy}$, is approximated by a cylindrical volume of height h and radius r_{xy} in case c.

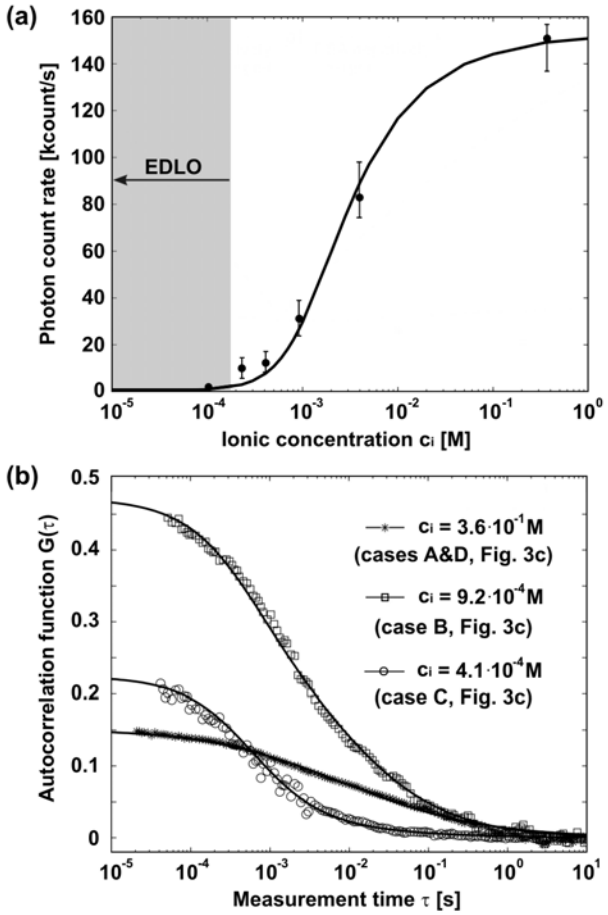

Figure 2. Measurements of fluorescent proteins. (a) Photon count rate of 50nM WGA at different ionic strengths c_i in a 50nm high nanochannel. The dots are experimental measurements whereas the line is a fitting obtained with equation 8. Pyrex surfaces are negatively charged, which excludes negatively charged WGA proteins from the nanochannel. When electrical double layer overlap (EDLO) occurs, a total exclusion of proteins from the nanochannel can be seen. (b) Autocorrelation functions of fluorescence fluctuations of 38 kDa Wheat Germ Agglutinin with Alexa Fluor® 633 in a 50nm high nanochannel for solutions of different ionic concentration at pH = 7. Fitting using equation 16 with τ_{bulk} = 0.6ms, τ_{surf} = 10ms and α = 0.45 as fixed parameters gives N_{bulk} = 0.2 and N_{surf} = 5.4 for $c_i = 3.6 \cdot 10^{-1}$M, N_{bulk} = 0.5 and N_{surf} = 0.6 for $c_i = 9.2 \cdot 10^{-4}$M and N_{bulk} = 0.9 and N_{surf} = 0.1 for $c_i = 4.1 \cdot 10^{-4}$M.

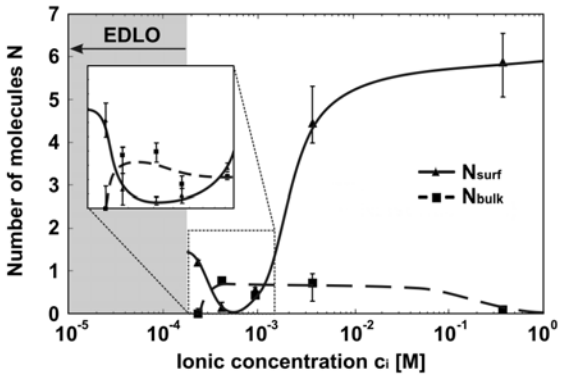

Figure 3. Number of WGA proteins diffusing in a 50nm high nanochannel, at different ionic strengths, obtained by fitting the autocorrelation functions with eq 16. N_{bulk} represents the number of molecules which do not interact with the surfaces (τ_{bulk} = 0.6±0.02ms) and N_{surf} represents the molecules which interact with surfaces and get retarded (τ_{surf} = 10±2ms, α = 0.45±0.1). Experimental data were performed at pH = 7 and are represented by marks; lines are plotted by interpolating these data in order to guide the eye of the reader.

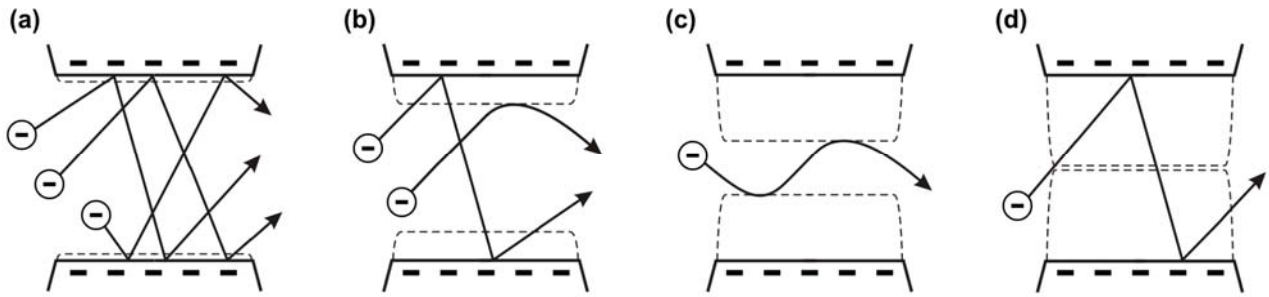

Figure 4. Schematics of the typical behavior of negatively charged biomolecules inside a nanochannel with negatively charged surfaces, at different ionic strengths. Our model is based on 2 different populations of molecules: the molecules which never touch the pore walls (N_{bulk}, τ_{bulk}) and those which adsorb on the surfaces and get retarded (N_{surf}, τ_{surf}). a) at high ionic concentrations, the electrical double layer (EDL, represented by a dashed line) is thin and does not prevent most molecules to interact with the surfaces ($N_{bulk} \rightarrow 0$). b) when the ionic concentration decreases, the EDL increases and some molecules do not interact with the surfaces any more. As the EDL increases, the number of molecules interacting with the surfaces decreases. c) when the EDL is large enough, most of the molecules do not interact with the surfaces ($N_{surf} \rightarrow 0$). d) when the channel is just not closed by the EDL, very few molecules enter in the channel and interact again with the surfaces.

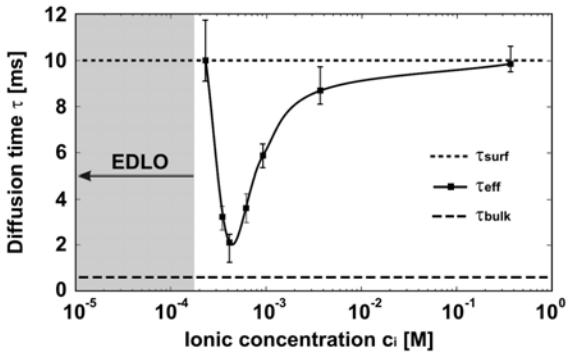

Figure 5. Effective diffusion times for WGA proteins in a 50nm high nanochannel at different ionic strengths. Marks represent the effective diffusion times calculated with equation 13 from measurements of figure 3. The line is plotted by interpolating these data in order to guide the eye of the reader. The dotted and dashed lines represent the values of the fixed parameters τ_{bulk} = 0.6ms and τ_{surf} = 10ms.